SCIENCE CHINA
Earth Sciences

• RESEARCH PAPER •

September 2015 Vol.58 No.9: 1623–1632
doi: 10.1007/s11430-015-5127-1

Upper ocean response to tropical cyclone wind forcing: A case study of typhoon Rammasun (2008)

PEI YuHua[1,2], ZHANG RongHua[3] & CHEN DaKe[2*]

[1] *College of Physical and Environmental Oceanography, Ocean University of China, Qingdao 266100, China;*
[2] *State Key Laboratory of Satellite Ocean Environment Dynamics, Second Institute of Oceanography, State Oceanic Administration, Hangzhou 310012, China;*
[3] *Key Laboratory of Ocean Circulation and Waves, Institute of Oceanology, Chinese Academy of Sciences, Qingdao 266071, China*

Received January 28, 2015; accepted May 15, 2015; published online June 29, 2015

The characteristics of the upper ocean response to tropical cyclone wind (TCW) forcing in the northwestern Pacific were investigated using satellite and Argo data, as well as an ocean general circulation model. In particular, a case study was carried out on typhoon Rammasun, which passed through our study area during May 6–13, 2008. It is found that the local response right under the TCW forcing is characterized by a quick deepening of the surface mixed layer, a strong latent heat loss to the atmosphere, and an intense upwelling near the center of typhoon, leading to a cooling of the oceanic surface layer that persists as a cold wake along the typhoon track. More interestingly, the upper ocean response exhibits a four-layer thermal structure, including a cooling layer near the surface and a warming layer right below, accompanied by another pair of cooling/warming layers in the thermocline. The formation of the surface cooling/warming layers can be readily explained by the strong vertical mixing induced by TCW forcing, while the thermal response in the thermocline is probably a result of the cyclone-driven upwelling and the associated advective processes.

tropical cyclone wind forcing, upper ocean response, satellite and Argo data, ocean modeling

Citation: Pei Y H, Zhang R H, Chen D K. 2015. Upper ocean response to tropical cyclone wind forcing: A case study of typhoon Rammasun (2008). Science China: Earth Sciences, 58: 1623−1632, doi: 10.1007/s11430-015-5127-1

Tropical cyclones (TCs), also known as typhoons in the western North Pacific or hurricanes in the Atlantic and the eastern Pacific, are severe storms exerting strong wind forcing to the ocean. The effects of tropical cyclone wind (TCW) on large-scale ocean state and low-frequency climate variability have recently aroused an increased interest as debates continue about the relationships between TC activity and global warming. While conditions disturbed by TCs in the atmosphere are restored quickly (a couple of days) after TC passage, those in the ocean can persist for weeks and longer. It has been shown that the synoptic-scale TCs can have significant climatic and global impact (Emanuel, 1987, 2001; Henderson-Sellers et al., 1998; Webster et al., 2005; Pasquero and Emanuel, 2008; Korty et al., 2008; Hu and Meehl, 2009; Jansen and Ferrari, 2009; Chen and Tam, 2010), and that TCW forcing can largely alter the thermal conditions in the Pacific (Sriver and Huber, 2007, 2010; Fedorov et al., 2010; Sriver et al., 2010; Kim et al., 2011). In particular, it is found that TCW forcing over the western Pacific can have a remote effect on the eastern equatorial Pacific Ocean (Zhang et al., 2013).

To explore the role of TCs in the climate system, we need to understand the characteristics of the local oceanic response to TCs and the related physical processes. As shown by many previous studies (Price, 1981; Jacob et al.,

*Corresponding author (email: dchen@sio.org.cn)

2000; Ginis, 2002; Lin et al., 2003; Price et al., 2008; Zedler, 2009; Huang et al., 2009; Vincent et al., 2012), the most prominent response is characterized by a cooling of the sea surface temperature (SST), and the entrainment of cold water from below is identified as the major process responsible for the cooling. The advent of satellite and Argo observations have led to significant advances in our understanding, interpretation and modeling of the ocean response and feedback to TCs (Lin et al., 2003; Wu and Chen, 2012). Satellite-based wind and SST data can be used to characterize TC forcing and sea surface response, while Argo profiles can reveal the vertical structure of the upper ocean response to TCs.

Despite the tremendous progress in our understanding of the ocean response to TCs, the explanations of the response mechanisms are still in debate. Various processes (e.g., Ekman pumping, vertical mixing and surface heat and freshwater exchanges) have been shown to be important, but their relative roles remain elusive. This is partly due to the lack of detailed *in situ* observations of the ocean-TC interaction. In addition, satellite-based observational descriptions are limited to the surface, while Argo-based data analyses suffer from relatively low spatial and temporal resolutions. At present, there is no way to fully decipher the mechanisms of ocean response to TC based on observations alone.

Numerical modeling has been a powerful approach to study ocean response to TC, and have greatly improved our understanding of the basic physical processes involved. However, different models still exhibit considerable discrepancies as compared to one another and to observed features of the upper ocean response. Model results are sensitively dependent on a variety of factors, including model formulations, experiment settings, the way the wind forcing is represented, the background ocean state, and the parameterizations of sub-grid processes. Of particular importance for simulating the upper ocean response to TC are well-resolved and parameterized vertical mixing processes. Thus in this study we use an ocean general circulation model (OGCM) that has a special vertical coordinate to resolve the ML variability (Gent and Cane, 1989) and a vertical mixing scheme that captures the main turbulent mixing processes in the upper ocean (Chen et al., 1994).

Our intention here is to investigate the characteristics and structures of the upper ocean response to TCs with a case study of typhoon Rammasun (2008), based on numerical model experiments as well as observational data.

1 Data and model

1.1 Satellite and Argo observations

Satellite observed wind data are used to extract the TCW forcing for the model. The data are from the Cross-Calibrated Multi-Platform (CCMP) ocean surface wind product (Atlas et al., 2011), which are available at podaac.jpl.nasa.gov from July 1987 to December 2011, with a horizontal resolution of 0.25°×0.25°, and a 6-hourly temporal resolution at 0, 6, 12, 18 Z of a day.

Typhoon Rammasun is tracked by the "best track" data from the U.S. Joint Typhoon Warning Center (JTWC, www.usno.navy.mil/JTWC) (Chu et al., 2002). The dataset contains time series of the TC center position and intensity at 6-hour interval over the lifetime of each TC, with the intensity being represented by the maximum sustained 1-min mean 10-m wind speed.

Satellite and Argo temperature data are used to depict the characteristics of the upper ocean thermal response to typhoon Rammasun, and also to validate the model results. SST data are from the Tropical Rainfall Measuring Mission (TRMM) microwave imager (TMI) measurements, produced by Remote Sensing Systems (available at www.remss.com), which are available daily from December 1997 to the present with a spatial resolution of 0.25°×0.25°. The Argo profiles used in this study are provided by China Argo Real-time Data Center (available at www.argo.org.cn).

1.2 The ocean model

The OGCM used in this work is a reduced-gravity, primitive-equation, sigma-coordinate model developed by Gent and Cane (1989). The vertical structure of the model consists of a mixed layer (the first layer) and a number of layers below that are specified according to a sigma-coordinate. Several efforts have been devoted to improving this model, including parameterizing the vertical mixing with a hybrid mixing scheme (Chen et al., 1994), representing the surface freshwater flux as a natural boundary condition (Murtugudde and Busalacchi, 1998), and simulating the penetrative radiation with an attenuation depth (H_p) derived from satellite ocean color data (Murtugudde et al., 2002). An advective atmospheric mixed layer model is incorporated into the OGCM to estimate surface heat fluxes (Murtugudde et al., 1996), which accounts for the non-local effect on SST by the atmospheric boundary layer and allows for a realistic representation of the feedbacks between the ocean and the atmosphere (Seager et al., 1995).

The model domain covers the tropical Pacific basin from 120°E to 76°W and from 25°S to 25°N, with a horizontal resolution of 0.33° in longitude and 0.23°–0.72° in latitude, and 25 layers in the vertical. Sponge layers are imposed near the southern and northern boundaries (poleward of 20°S/N) to damp out unwanted signals and relax the model state to climatology. The model is initialized from the WOA01 temperature and salinity fields (Levitus et al., 2005), and is integrated for 20 years (the spin-up run) using prescribed monthly-mean climatological atmospheric forcing fields, including the reanalysis wind stress fields from the European Center for Medium-Range Weather Forecasts (Hackert et al., 2001), the solar radiation from the Earth

Radiation Budget Experiment, the cloudiness from the International Satellite Cloud Climatology Project, and the precipitation from Xie and Arkin (1995). Note that during the spin-up run there is no TCW forcing, which is added later using the satellite wind data and the Loess method described below.

Figure 1 is an illustration of the modeling strategy used in this work, consisting of a basin-scale OGCM of the tropical Pacific forced by either the climatological forcing or the TCW forcing superimposed on the climatology. In the latter case, the total wind stress (τ) consists of a climatological part (τ_{clim}) and a TC-induced part (τ_{TC}). Using the same modeling system but with a lower horizontal resolution, Zhang et al. (2013) have recently shown that the TCW forcing over the western tropical Pacific can induce significant remote response in the eastern equatorial Pacific Ocean where the mixing and upwelling are strong, and the thermocline is shallow.

1.3 The Loess method used to extract TCW forcing

In order to explicitly extract the TCW signal from satellite wind data, a locally weighted quadratic least-squares regression (Loess) method is utilized (O'Neill et al., 2010). Specifically, the smoothed value ($\bar{A}$) of a field (A) at a grid point is estimated by fitting a regression surface to some subset data locally. Then, a perturbation field is obtained as $A' = A - \bar{A}$. As detailed in O'Neill et al. (2010), the so-called half span parameters, denoted as α_x and α_y in x and y directions, respectively, are introduced in the Loess method to indicate how much of the subset data is used to fit each quadratic regression locally. The resulting perturbation fields depend on these two parameters. The larger the values of α_x and α_y, the smoother the $\bar{A}$ field, and the stronger the perturbation fields (A').

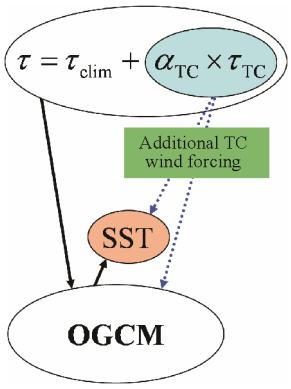

Figure 1 A schematic showing an ocean general circulation model with TC-induced wind forcing explicitly taken into account. The total wind stress used to force the ocean is separated into its climatological part (τ_{clim}) and TC part ($\alpha_{\text{TC}} \times \tau_{\text{TC}}$), where α_{TC} is a scalar parameter introduced to represent the intensity of TCW forcing.

1.4 Model experiment design

Figure 2 shows the track of typhoon Rammasun observed on May 6–13, 2008. Rammasun was formed on May 5 as a tropical disturbance, intensified to a tropical storm on May 7, upgraded to a typhoon on May 9, and became a category 4 super-typhoon on the Saffir-Simpson hurricane wind scale on May 10, with its peak winds reaching 135 knots. After that, Rammasun weakened gradually and downgraded to a tropical storm on May 12.

Figure 3 shows a snapshot of the satellite-observed total wind stress field at 0 Z on 10 May 2008, as well as the TC wind stress fields extracted using the Loess filter with two different sets of parameters. Obviously, the structure and amplitude of the TC winds are sensitive to the half-span parameters α_x and α_y. We opt for α_x = 6° and α_y = 6° to better resolve the inner core of the TC, and adjust the coefficient α_{TC} (see Figure 1) to rescale the TC to observed intensity. Furthermore, we define the influence area of TCW as a circle centered on the TC track with a 6° radius and set the wind field outside of this area to zero.

Figure 4 displays the daily-mean τ_{TC} calculated for May 9, 2008 from 125°E to150°E at 11°N with different intensity coefficient α_{TC}. The Loess method captures the structure of the typhoon-induced wind forcing effectively, including the calm "eye" at the center of Rammasun, and the asymmetric structure of the maximum sustained wind stress around the eye. As compared to the directly observed

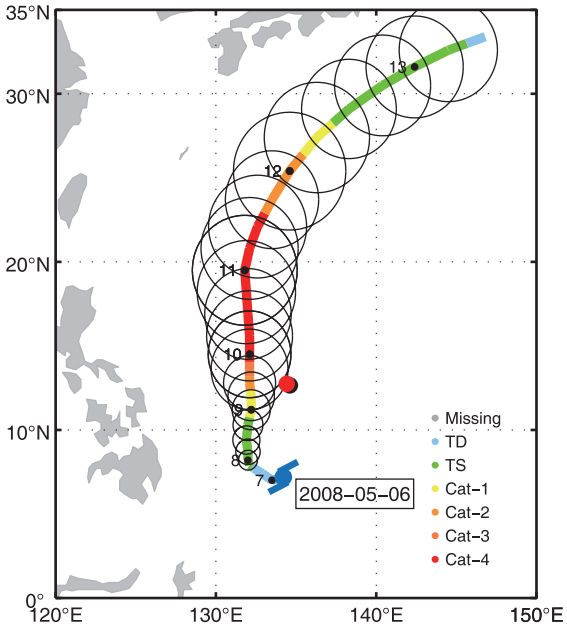

Figure 2 Rammasun's track and intensity (on Saffir-Simpson hurricane wind scale) observed over the northwestern Pacific during May 6–13, 2008. The black circles represent the radius of 34 knot (17 m s^{-1}) maximum sustained wind R_{17} at 6-hour intervals. The numbers along the track denote the dates in May, 2008. The black and red overlapping dots denote the locations (black: 134.6°E, 12.6°N on May 4; red: 134.4°E, 12.7°N on May 14) of the Argo profile pair in Figure 8(a).

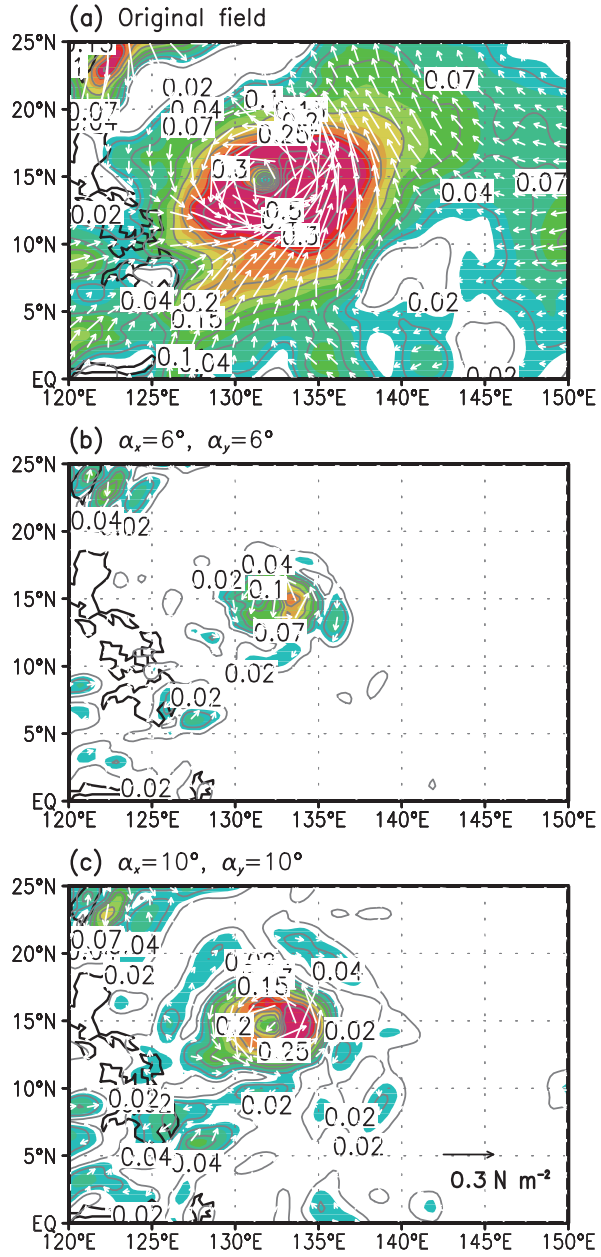

Figure 3 Wind stress fields from satellite measurements at 0 Z on 10 May 2008. (a) The original CCMP field; (b) Rammasun's wind stress extracted using the Loess filter with the half-span smoothing parameters $\alpha_x = 6°$ and $\alpha_y = 6°$; (c) the same as (b) but for $\alpha_x = 10°$ and $\alpha_y = 10°$.

CCMP wind stress, the derived τ_{TC} shows a better intensity match when taking $\alpha_{TC} = 3.0$; therefore we use $\tau = \tau_{clim} + 3\tau_{TC}$ for the standard model run.

2 Upper ocean response to typhoon Rammasun

Two experiments are performed using the OGCM (Figure 1), started from the same spin-up run. One is referred to as the no-TCW run in which the τ_{TC} part is not included ($\alpha_{TC} = 0.0$); the other is referred to as the standard TCW run, in

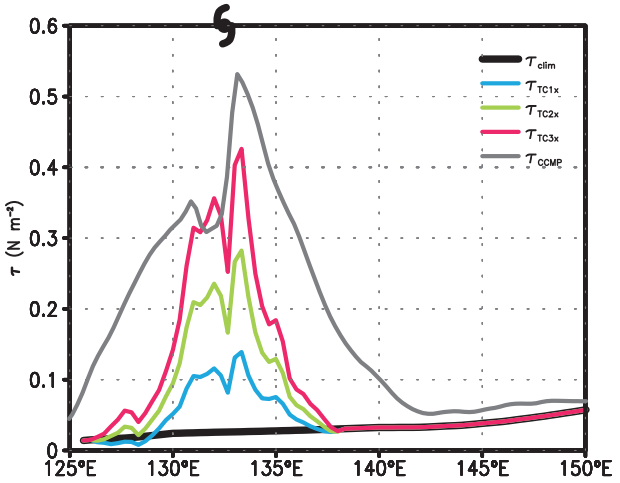

Figure 4 The amplitude of daily-mean wind stress from 125°E to150°E at 11°N on May 9, 2008. The black line indicates the prescribed climatological wind stress τ_{clim} for the control run, the grey line represents the daily-mean wind stress from the CCMP satellite measurements, and the blue, green, red lines are wind stress forcing $\tau_{clim} + \tau_{TC}$, $\tau_{clim} + 2\tau_{TC}$, $\tau_{clim} + 3\tau_{TC}$ for TC-1x, TC-2x, TC-3x model runs, respectively.

which the $\alpha_{TC} \times \tau_{TC}$ part ($\alpha_{TC} = 3.0$ and $\alpha_x = \alpha_y = 6°$) is explicitly incorporated, with other model settings being kept exactly the same as in the no-TCW run. The OGCM is initialized from May 1, 2008, integrated for a month for both runs, whose differences are calculated as the effects induced by the prescribed TCW forcing. While the atmospheric conditions disturbed by typhoon Rammasun restored very quickly (a couple of days) after typhoon passage, the large perturbations in the ocean persisted for weeks and longer. Here satellite-based SST data and Argo data are combined with model simulations to reveal the characteristics of the upper ocean response to typhoon Rammasun during May 6–13, 2008.

2.1 SST response

To depict the SST response to Rammasun, the observed daily TMI SST changes (ΔSST_{TMI}) are calculated as the differences from that on May 3, 2008, a date considered to represent pre-typhoon condition. For the model simulations, the SST changes (ΔSST_{OGCM}) are calculated as the differences between the TC runs and the climatology run.

Figure 5 displays the spatial patterns of observed SST response to Rammasun on May 9–12, 2008. It is seen that the TCW forcing induced a large-scale SST cooling around its track, with a magnitude as large as 4°C. The negative SST anomalies exhibited relatively quick recovery for the first week after Rammasun's passage, and were restored slowly thereafter. The total recovery time of the SST cooling is more than one month, as shown in Figure 6, which presents the time series of the observed SST response averaged in the area (130°E–135°E, 5°N–10°N). In addition, the spatial scales of the SST perturbations were larger than that

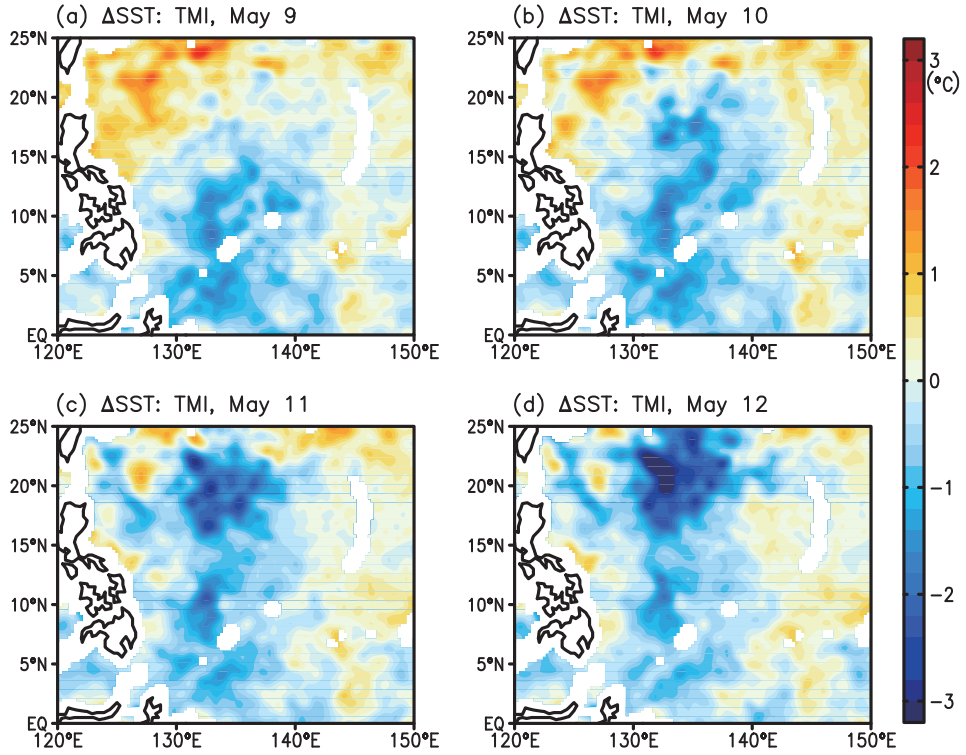

Figure 5 Rammasun induced daily-mean SST response from the TMI measurements on May 9–12, 2008. The response is calculated relative to the pre-typhoon condition on May 3, 2008. The color contour interval is 0.2°C.

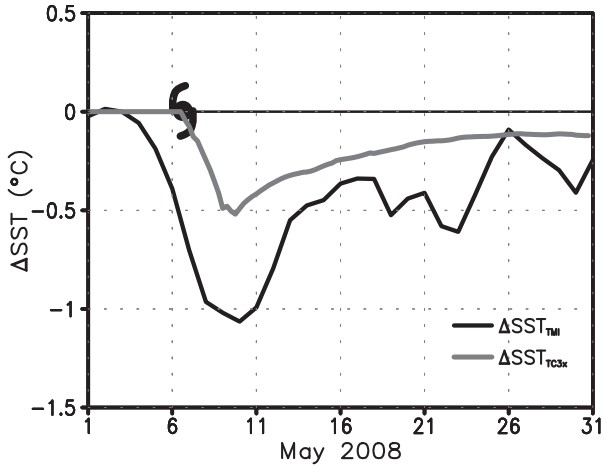

Figure 6 Time series of ΔSST averaged in the area (130°E–135°E, 5°N–10°N). The black and grey lines indicate ΔSST observed by TMI and modeled in the standard TC run, respectively.

of the TCW forcing (Figure 3).

Figure 7 shows the spatial patterns of the simulated SST response to Rammasun from May 9 to May 12, 2008. Consistent with the observed SST response (Figure 5), a cold wake emerged after Rammasun's passage. On May 9, a significant cooling appeared in the region between 130°E to 135°E and 5°N to 10°N, similar to that observed by satellite. As Rammasun passed by, the SST cooling followed the typhoon's track. On May 12, the modeled SST cooling was as large as 2°C, with the largest cooling area being shifted to the north of 20°N (Figure 7(d)). The TCW-induced cooling was recovering as Rammasun moved away, but was not completely restored to the pre-typhoon condition, which implies that the TC-induced SST perturbations can persist in the ocean for a long time and may produce significant remote influences.

The time series of the model-simulated SST response to Rammasun is also shown in Figure 6 for the area (130°E–135°E, 5°N–10°N). The area-averaged SST cooling in the model appeared on May 7, and reached its maximum of 0.5°C on May 9, whereas the observed cooling appeared earlier with a maximum of 1.1°C. Consistent with the observation, the recovery of the modeled SST cooling was relatively quick in the first week after typhoon passage, but slowed down thereafter.

As evident in Figures 5–7, the SST response in the model simulation agrees qualitatively with that observed, but exhibits a much smoother evolution and weaker cooling amplitude. For example, the modeled largest cooling was 1.4°C at 24°N, while that observed by satellite was nearly 3°C. One might speculate that these discrepancies were caused by an underestimate of the actual wind field, which could have more complicated spatial and temporal variations aside from the "clean" TCW forcing extracted from the observations using the Loess filter. We will have more discussion on this later.

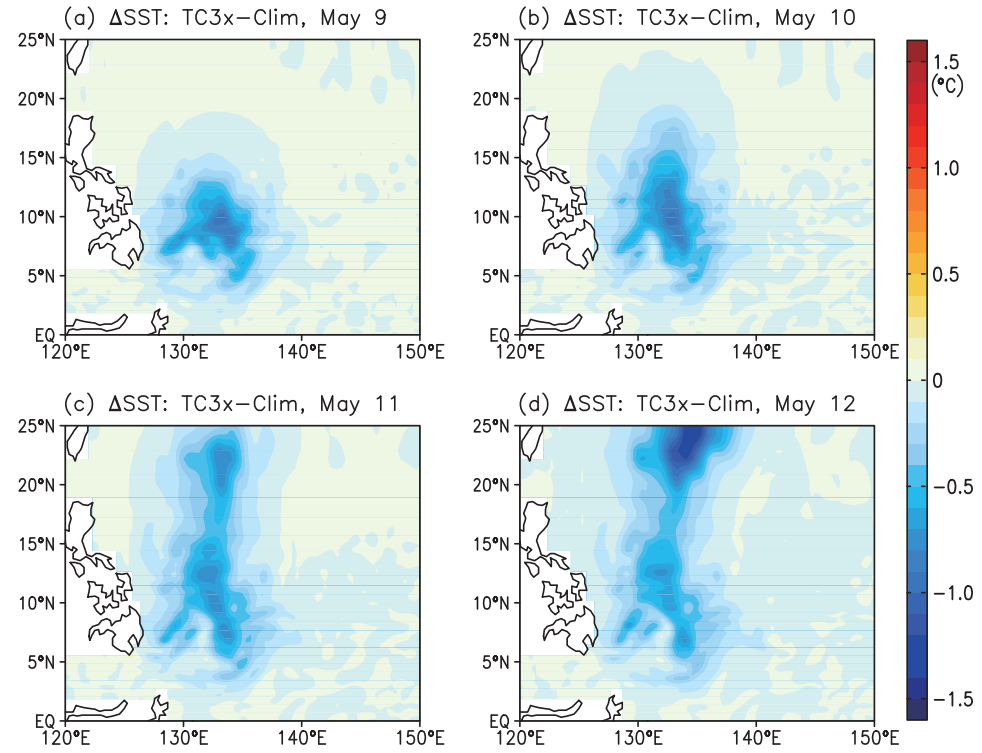

Figure 7 Rammasun induced daily-mean SST response from the standard model run (α_{TC} = 3.0) on May 9–12, 2008. The response is calculated as the difference between the standard run and the climatological run. The color contour interval is 0.1°C.

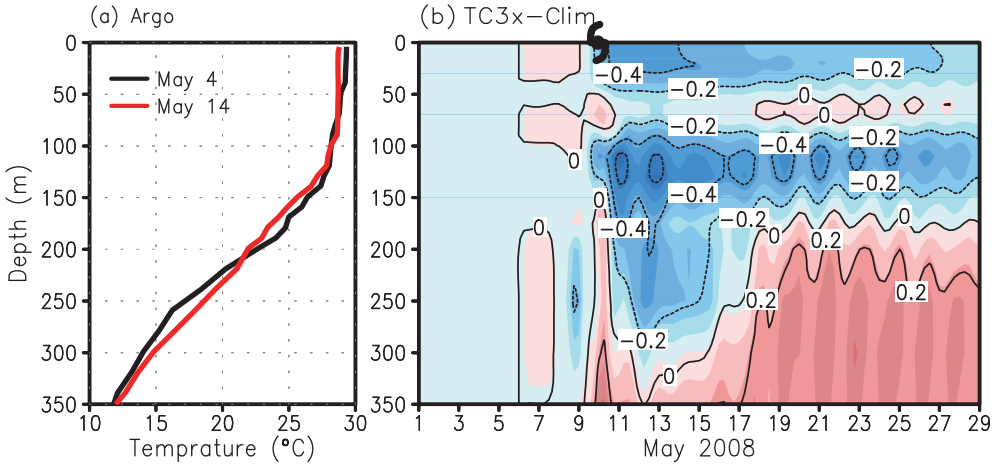

Figure 8 Vertical temperature changes during the passage of Rammasun. (a) Temperature profiles from Argo at (134.6°E, 12.6°N) on May 4 and (134.4°E, 12.7°N) on May 14, indicating conditions before and after Rammasun passage. (b) The evolution of the upper ocean temperature anomalies from the OGCM in May 2008 at (134.4°E, 12.7°N). The contour interval is 0.2°C in (b).

2.2 Thermal structure response

The ocean response is not limited to the surface but extends well to the subsurface depths. Figure 8(a) shows an example of observed changes of the upper ocean thermal structure in response to Rammasun, as measured by a pair of Argo temperature profiles obtained at 134.6°E, 12.6°N on May 4, and at 134.4°E, 12.7°N on May 14, 2008, respectively (as marked in Figure 2). A complicated multi-layer structure is seen in the vertical, with a cooling in the surface layer accompanied by a warming right below, and another two layers of cooling/warming in the thermocline. For comparison, Figure 8(b) shows the evolution of the model simulated vertical temperature anomalies at the same location. The observed multi-layer thermal response is well reproduced in the model.

The changes in the vertical thermal structure are caused by the TC-induced surface mixing and subsurface advection, and they in turn can modify the density stratification and further affect the mixing and advective processes in the

ocean. As these cooling and warming signals in the upper ocean persist for weeks and longer, they can be brought away from the source regions to other areas where no TC wind forcing is directly present, thus modulating the ocean circulation and heat balance. For example, as demonstrated by Zhang et al. (2013), the TCW forcing in the western off-equatorial Pacific could have a basin-wide impact, causing significant perturbations even in the eastern equatorial Pacific.

2.3 Mixed layer depth response

The surface mixed layer depth (MLD) deepening is a commonly observed feature of the upper ocean response to TC (Wu and Chen, 2012). Figure 9 shows the spatial distribution of the model simulated MLD response on May 9–12, 2008. Note that the MLD in our model is explicitly computed using a hybrid vertical mixing scheme (Chen et al., 1994). As indicated in Zhang et al. (2013), the mean structure of the MLD over the western tropical Pacific is well simulated in this model as compared with that from observational data.

As seen in Figure 9, a pattern of the MLD deepening followed the center of typhoon Rammasun closely. In the region directly exposed to Rammasun, there was a significant local deepening with its daily-mean magnitude being over 50 m, which is consistent with the profile change seen in Argo data. Different from the SST response which left a sustained cooling in Rammasun's wake, the MLD deepening recovered quickly, and a MLD shoaling appeared in the wake of the typhoon, which is due to the restratification forced by the enhanced surface heat input after typhoon passage, as we will see later.

3 Heat budget analysis

3.1 Surface heat flux

In association with the SST cooling, a negative heat flux (i.e., out of the ocean) is seen at the sea surface (Figure 10(a)). Over the central area influenced by Rammasun, there was about 200 W m^{-2} heat going out of the ocean on May 9, 2008, which acted to cool the ocean surface by more than 0.1°C per day (Figure 10(a)). The surface heat loss followed Rammasun closely, but there was a heat gain in the wake of typhoon. In other words, the surface heat flux changes sign from being negative during the direct TC influence to being positive after the TC passage, thus acting to enhance the SST cooling under the TCW forcing, and to restore SST and reduce MLD afterwards. Further analyses indicate that the heat loss under the TCW forcing was mostly attributable to the enhanced latent heat flux, while the effects of the sensible and radiative fluxes were relatively small (figures not shown). In the cold wake of the typhoon, however, the downward sensible heat flux was responsible for the heat input that would eventually restore the SST change. It seems likely that the TCW-induced SST

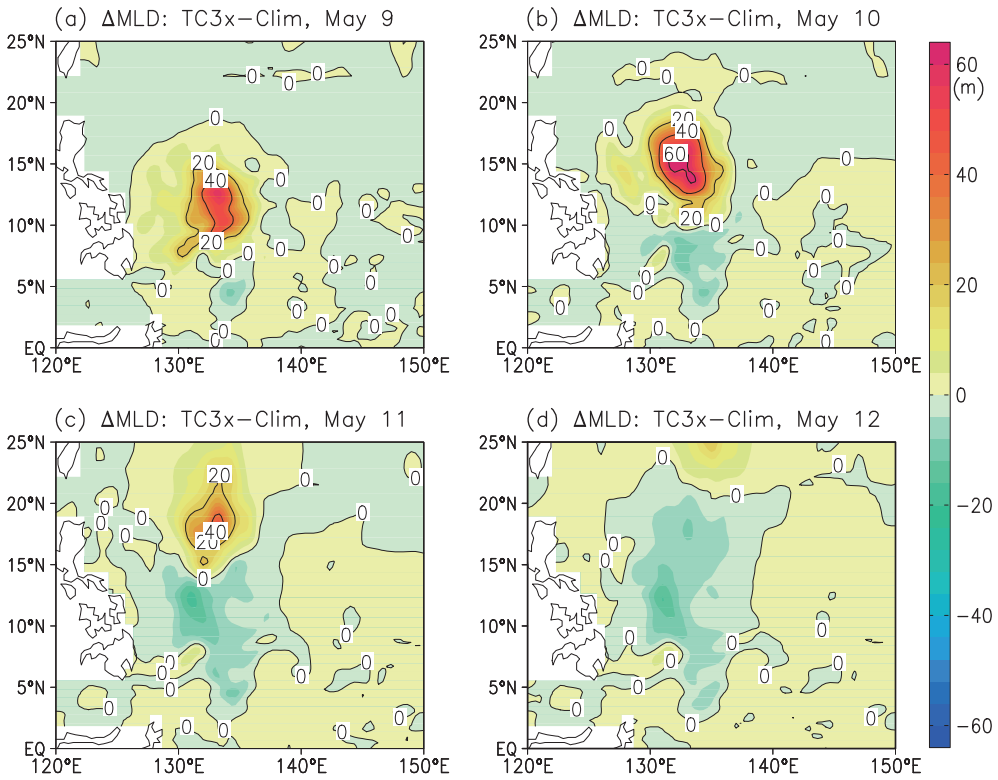

Figure 9 Rammasun induced daily-mean MLD changes on May 9–12, 2008 from the standard model run. The shaded color interval is 4 m.

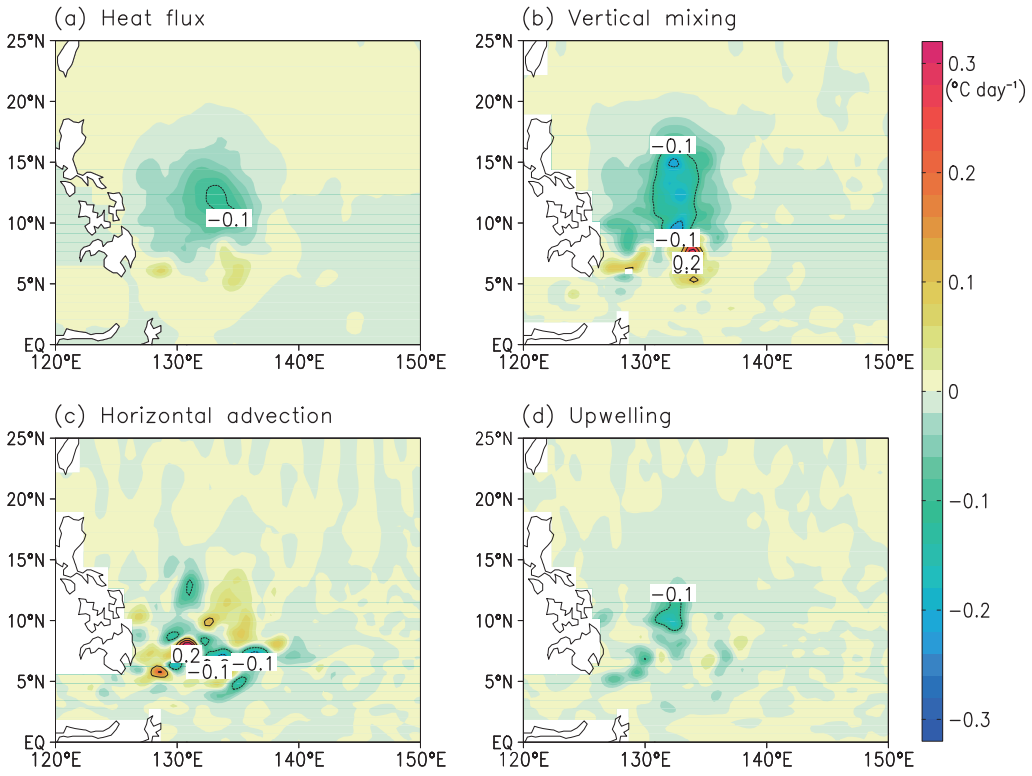

Figure 10 The anomalous mixed layer heat budget on May 9, 2008 from the standard model run. (a) Net surface heat flux, (b) vertical mixing, (c) horizontal advection, (d) upwelling. The color interval is 0.02°C day^{-1}.

cooling can be attributed to the combined effects of the surface latent heat loss and the oceanic processes, while the recovery of such a cooling depends on the sensible heat gain after the TC passage.

3.2 Mixed layer heat budget

To further understand the processes by which the cooling is induced by the TCW forcing, a heat budget analysis is performed for the surface mixed layer. Figure 10 displays the spatial distributions of the heat budget terms, including surface heat flux, vertical mixing, zonal and meridional advection, and upwelling in the standard model run. It is clear that the vertical mixing (Figure 10(b)) (~65%) and the surface heat flux (Figure 10(a)) (~35%) were two dominant cooling terms in the heat budget, while horizontal advections were relatively small and less coherent. Upwelling (Figure 10(d)) also contributed significantly to the heat budget near the center of Rammasum, where the vertical mixing (~60%), heat flux (~20%), and upwelling (~20%) together produced the intense surface cooling.

Therefore, the local response of the upper ocean to the TCW forcing is characterized by a quick deepening of MLD, a strong latent heat loss, an intense upwelling near the center of typhoon, and thus a cooling of SST that persists as a cold wake along the typhoon track. After the typhoon moves away, the ocean starts to gain heat through sensible heat flux, leading to a quick shoaling of MLD and a gradual recovery of SST. Note that the spatial scale of the perturbed fields in the ocean is larger than that of the prescribed TCW forcing, indicating the non-local effects of the TCW forcing on the upper ocean.

4 Sensitivity experiments

The sensitivity of the model simulation to the specification of the wind forcing are evaluated by changing the coefficient α_{TC} of the TCW forcing, and by applying the original CCMP wind forcing without filtering (Table 1). The differences in strength and size of these wind forcings have been shown in Figure 4 for typhoon Rammasun along a section at 11°N on May 9, 2008. Figure 11 compares the modeled SST responses to these different wind forcings along the same section on May 10, 2008, when the SST cooling reached a maximum. Evidently, the observed SST anomalies are large and highly variable in space, while those produced by all model simulations are smaller and confined to the central region of Rammasun.

As expected, the larger the value of α_{TC}, the stronger the upper ocean response, while the spatial patterns of the response with different α_{TC} are qualitatively similar to one another. Quantitatively, for α_{TC}=1.0, 2.0 and 3.0, the maximum SST cooling at this location was –0.6°C, –1.3°C and –1.5°C; the surface heat loss was –260 W m^{-2}, –360 W m^{-2}, and –460 W m^{-2}; and the mixed layer deepening was 50, 70,

Table 1 The model experiments with different wind forcing [a)]

Numerical experiments	Model forcing
Control run	τ_{clim}
TC-1x run	$\tau_{clim} + \tau_{TC}$
TC-2x run	$\tau_{clim} + 2\tau_{TC}$
TC-3x run	$\tau_{clim} + 3\tau_{TC}$
TC-ccmp run	τ_{CCMP}

a) τ_{clim} is the climatological wind stress, τ_{TC} is the TC wind stress extracted from the CCMP satellite observations, and τ_{CCMP} is the original CCMP wind stress.

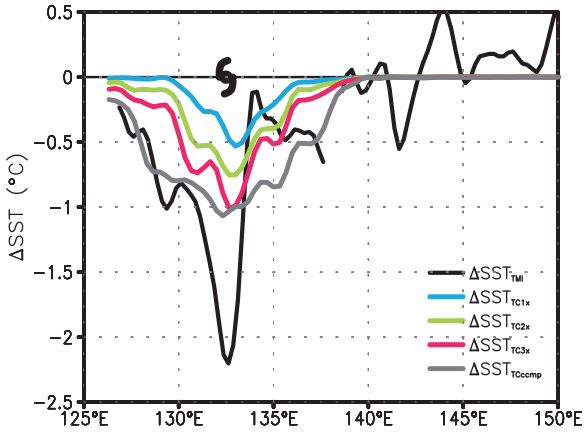

Figure 11 SST perturbations (ΔSST) induced by typhoon Rammasun from 125°E to 150°E at 11°N on May 10, 2008. The black solid line is the ΔSST observed by TMI. The grey line is the ΔSST from the model run directly forced by the CCMP winds. The color lines are the ΔSST from the model runs with different α_{TC}.

and 75 m, respectively. Forcing the model with the original CCMP wind field did not increase the maximum SST cooling from the standard run ($\alpha_{TC} = 3.0$), but largely broadened the region of cooling. It seems that the mismatch between the model simulations and the observation cannot be simply attributed to the specification of wind forcing. The large spatial oscillation of the observed SST anomalies suggests a strong influence of oceanic eddies, which is absent in our coarse-grid model simulations.

5 Concluding remarks

In this study, a series of ocean model experiments are combined with satellite and Argo observations to evaluate the upper ocean response to the TCW forcing in the western tropical Pacific, with particular emphasis on typhoon Rammasun. It is found that the local response right under the TCW forcing is characterized by a quick deepening of the surface mixed layer, a strong latent heat flux to the atmosphere, an intense upwelling near the center of typhoon, and thus a cooling of the oceanic surface layer that persists as a cold wake along the typhoon track. After the typhoon moves away, the ocean starts to gain heat through surface sensible heat flux, leading to a quick shoaling of the mixed layer and a gradual restoration of the surface thermal condition.

An interesting finding of this study is the multi-layer temperature anomalies of the upper ocean in response to typhoon. Consistent with the changes of Argo temperature profiles, the model response forced by the TCW exhibits a four-layer thermal structure, including a cooling layer near the surface and a warming layer right below, accompanied by another pair of cooling/warming layers in the thermocline. The formation of the surface cooling/warming layers can be readily explained by the strong vertical mixing induced by TCW forcing, which is the essence of the "heat pump" theory of TC's impact on the ocean (Emanuel, 2001). On the other hand, the thermal response in the thermocline is probably a result of the flow convergence and thus upwelling/downwelling in the thermocline, due to the suction effect of the cyclonic wind forcing. This point needs to be further verified.

Through a mixed layer heat budget analysis, we demonstrated that the SST cooling under typhoon can be attributed to the combined effect of the vertical mixing, the latent heat loss and the upwelling near the center of typhoon, with the mixing playing a dominant role. It has long been recognized that the mixing and upwelling (especially mixing) are the most important processes responsible for the SST cooling under typhoon (Price, 1981), but the cooling effect of surface heat flux is usually considered negligible as compared to that of the oceanic processes. The unusually large contribution of the surface heat flux (Figure 10) in our analysis suggests that the latent heat loss associated with the strong TCW could play a significant role in cooling SST for fast-moving typhoons such as Rammasun.

The results of this study are considered preliminary and obvious limitations exist in this ocean-only modeling effort. Despite the qualitative agreement between the simulated and observed characteristics of ocean response, there are sizable quantitative mismatches between the two, especially in terms of the magnitude and distribution of the surface cooling. This is mostly because our experiments are designed for a "clean" look at the processes involved in the upper ocean response to TC rather than a realistic simulation. The large spatial variability of the observed SST anomalies (Figures 5 and 11) indicates the possible influences of oceanic eddies and TC-eddy interactions. In order to better simulate the observed response and to elucidate the physical processes involved in more details, we need to employ an eddy-resolving model initialized with a realistic ocean state. This is our ongoing work and will be reported on another occasion.

We would like to thank A J Busalacchi, Su JiLan, and Zhang DaLin for their helpful comments, and D Chelton and L O'Neill for providing the Loess code. This work was supported by the National Basic Research Pro-

gram of China (Grant No. 2013CB430302), the National Natural Science Foundation of China (Grant Nos. 91128204, 41321004, 41475101, 41421005), the China Scholarship Council, the CAS Strategic Priority Project (Grant Nos. XDA 11010301, XDA11010104), and the National Natural Science Foundation of China-Shandong Joint Fund for Marine Science Research Centers (Grant No. U1406401). The TMI data are produced by Remote Sensing Systems (www.remss.com) and sponsored by the NASA Earth Science MEaSUREs DISCOVER Project. The CCMP wind data are available from NASA at http://podaac.jpl.nasa.gov/. We thank the two anonymous reviewers for their helpful comments.

Atlas R, Hoffman R N, Ardizzone J, Leidner S M, Jusem J C, Smith D K, Gombos D. 2011. A cross-calibrated, multiplatform ocean surface wind velocity product for meteorological and oceanographic applications. Bull Amer Meteorol Soc, 92: 157–174

Chen D, Rothstein L M, Busalacchi A J. 1994. A hybrid vertical mixing scheme and its application to tropical ocean models. J Phys Oceanogr, 24: 2156–2179

Chen G, Tam C Y. 2010. Different impacts of two kinds of Pacific Ocean warming on tropical cyclone frequency over the western North Pacific. Geophys Res Lett, 37: L01803, doi: 10.1029/2009GL041708

Chu J H, Sampson C R, Levine A S, et al. 2002. The Joint Typhoon Warning Center tropical cyclone best tracks, 1945-2000. Naval Research Laboratory Technical Report. NRL/MR/7540-02-16, 112

Emanuel K A. 1987. The dependence of hurricane intensity on climate. Nature, 326: 483–485

Emanuel K A. 2001. Contribution of tropical cyclones to meridional heat transport by the oceans. J Geophys Res, 106: 14771–14781

Fedorov A V, Brierley C M, Emanuel K A. 2010. Tropical cyclones and permanent El Niño in the early Pliocene epoch. Nature, 463: 1066–1070

Gent P R, Cane M A. 1989. A reduced gravity, primitive equation model of the upper equatorial ocean. J Comp Phys, 81: 444–480

Ginis I. 2002. Tropical cyclone-ocean interactions. In: Perrie W, ed. Atmosphere–Ocean Interactions. Boston: WIT Press. 83–114

Hackert E C, Busalacchi A J, Murtugudde R. 2001. A wind comparison study using an ocean general circulation model for the 1997–1998 El Niño. J Geophys Res, 106: 2345–2362

Henderson-sellers A, Zhang H, Berz G, Emanuel K, Gray W, Landsea C, Holland G, Lighthill J, Shieh S L, Webster P, and Mcguffie K. 1998. Tropical cyclones and global climate change: A post-IPCC assessment. Bull Amer Meteorol Soc, 79: 19–38

Hu A, Meehl G A. 2009. Effect of the Atlantic hurricanes on the oceanic meridional overturning circulation and heat transport. Geophys Res Lett, 36: L03702, doi: 10.1029/2008GL036680

Huang P, Sanford T B, Imberger J. 2009. Heat and turbulent kinetic energy budgets for surface layer cooling induced by the passage of Hurricane Frances (2004). J Geophys Res, 114: C12023, doi: 10.1029/2009JC005603

Jacob S D, Shay L K, Mariano A J, Black P G. 2000. The 3D oceanic mixed layer response to hurricane Gilbert. J Phys Oceanogr, 30: 1407–1429

Jansen M, Ferrari R. 2009. Impact of the latitudinal distribution of tropical cyclones on ocean heat transport. Geophys Res Lett, 36: L06604, doi: 10.1029/2008GL036796

Kim H M, Webster P J, Curry J A. 2011. Modulation of North Pacific tropical cyclone activity by three phases of ENSO. J Clim, 24: 1839–1849

Korty R L, Emanuel K A, Scott J R. 2008. Tropical cyclone-induced upper-ocean mixing and climate: Application to equable climates. J Clim, 21: 638–654

Levitus S, Antonov J, Boyer T. 2005. Warming of the world ocean, 1955–2003. Geophys Res Lett, 32: L02604, doi: 10.1029/ 2004GL021592

Lin I I, Liu W T, Wu C C, Chiang J C H, Sui C H. 2003. Satellite observations of modulation of surface winds by typhoon-induced upper ocean cooling. Geophys Res Lett, 30: 1131, doi: 10.1029/2002GL015674

Murtugudde R, Beauchamp J, McClain C R, Lewis M, Busalacchi A J. 2002. Effects of penetrative radiation on the upper tropical ocean circulation. J Clim, 15: 470–486

Murtugudde R, Busalacchi A J. 1998. Salinity effects in a tropical ocean model. J Geophys Res, 103: 3283–3300

Murtugudde R, Seager R, Busalacchi A. 1996. Simulation of tropical oceans with an ocean GCM coupled to an atmospheric mixed layer model. J Clim, 9: 1795–1815

O'Neill L W, Chelton D B, Esbensen S K. 2010. The effects of SST-induced surface wind speed and direction gradients on midlatitude surface vorticity and divergence. J Clim, 23: 255–281

Pasquero C, Emanuel K. 2008. Tropical cyclones and transient upper ocean warming. J Clim, 21: 149–162

Price J F. 1981. Upper ocean response to a hurricane. J Phys Oceanogr, 11: 153–175

Price J F, Morzel J, Niiler P P. 2008. Warming of SST in the cool wake of a moving hurricane. J Geophys Res, 113: C07010, doi: 10.1029/ 2007JC004393

Seager R, Blumenthal M B, Kushnir Y. 1995. An advective atmospheric mixed layer model for ocean modeling purposes: Global simulation of surface heat fluxes. J Clim, 8: 1951–1964

Sriver R L, Goes M, Mann M E, Keller K. 2010. Climate response to tropical cyclone-induced ocean mixing in an Earth system model of intermediate complexity. J Geophys Res, 115: C10042, doi: 10.1029/ 2010JC006106

Sriver R L, Huber M. 2007. Observational evidence for an ocean heat pump induced by tropical cyclones. Nature, 447: 557–580

Sriver R L, Huber M. 2010. Modeled sensitivity of upper thermocline properties to tropical cyclone winds and possible feedbacks on the Hadley circulation. Geophys Res Lett, 37: L08704, doi: 10.1029/ 2010GL042836

Vincent E M, Lengaigne M, Madec G, Vialard J, Samson G, Jourdain N C, Menkes C E, Jullien S. 2012. Processes setting the characteristics of sea surface cooling induced by tropical cyclones. J Geophys Res, 117: C02020, doi: 10.1029/2011JC007396

Webster P J, Holland G T, Curry J A, Chang H R. 2005. Changes in tropical cyclone number, duration, and intensity in a warming environment. Science, 309: 1844–1846

Wu Q, Chen D. 2012. Typhoon-induced variability of the oceanic surface mixed layer observed by Argo floats in the western north Pacific ocean. Atmos Ocean, 50 (supl): 4–14

Xie P, Arkin P A. 1995. An intercomparison of gauge observations and satellite estimates of monthly precipitation. J Appl Meteorol, 34: 1143–1160

Zedler S E. 2009. Simulations of the ocean response to a hurricane: Nonlinear processes. J Phys Oceanogr, 39: 2618–2634

Zhang R H, Pei Y, Chen D. 2013. Remote effects of tropical cyclone wind forcing over the western Pacific on the eastern equatorial ocean. Adv Atmos Sci, 30: 1507–1525